Mon. Not. R. Astron. Soc. **000**, 1–5 (2009) Printed 14 May 2009 (MN LATEX style file v2.2)

Radial-velocity study of the post-period minimum cataclysmic variable SDSS J143317.78+101123.3 with an electron-multiplying CCD

S. M. Tulloch[1,2⋆], P. Rodríguez-Gil[2,3] and V. S. Dhillon[1]
[1] *Department of Physics and Astronomy, University of Sheffield, Sheffield, S3 7RH, UK*
[2] *Isaac Newton Group of Telescopes, Apartado de Correos 321, Santa Cruz de La Palma, E-38700, Spain*
[3] *Instituto de Astrofísica de Canarias, Vía Láctea, s/n, La Laguna, E-38205, Santa Cruz de Tenerife, Spain*

Accepted . Received 2009

ABSTRACT
We present high time-resolution spectroscopy of the eclipsing cataclysmic variable SDSS J143317.78+101123.3 obtained with QUCAM2, a high-speed/low-noise electron-multiplying CCD camera. Littlefair et al. (2008) measured the mass of the secondary star in SDSS J143317.78+101123.3 using a light-curve fitting technique and obtained a value of $M_2 = 0.060 \pm 0.003$ M$_\odot$, making it one of the three first bona-fide detections of a brown-dwarf mass donor in a cataclysmic variable. In this paper we present a dynamical measurement supporting this important result. We measured the radial-velocity semi-amplitude of the white dwarf from the motion of the wings of the Hα emission line and obtained a figure of $K_1 = 34 \pm 4$ km s^{-1}, in excellent agreement with the value of $K_1 = 35 \pm 2$ km s^{-1} predicted by Littlefair et al.'s model.

Key words: binaries: close – binaries: eclipsing – stars: dwarf novae – novae, cataclysmic variables – stars: individual : SDSS J143317.78+101123.3

1 INTRODUCTION

Cataclysmic variables (CVs) are close binary stars in which a white-dwarf (WD) primary accretes material from an accretion disc fed by a red-dwarf secondary (see Hellier (2001) and Warner (1995) for reviews). Theory predicts that the mass transfer from the secondary to the primary is accompanied by a shortening of the orbital period. This is believed to continue until the secondary star drops below the hydrogen-burning limit ($\sim 0.08 M_\odot$) and becomes a degenerate, brown-dwarf like object, at which point the period begins to increase. Models show that up to 70% of all CVs in the Galaxy should have brown-dwarf secondary stars at the present time, yet not a single such object had been positively identified until the discovery by Littlefair et al. (2006) of a secondary star of mass $M_2 = 0.052 \pm 0.002 M_\odot$ in the CV SDSS J103533.03+055158.4. Since then, two more brown-dwarf mass donors have been discovered by Littlefair et al. (2008) SDSS J150137.22+550123.3 and SDSS J150722.30+523039.8 and it now appears as if the missing population of post-period minimum CVs has finally been identified.

The results of Littlefair et al. (2008) and Littlefair et al. (2006) rely on an eclipse light-curve fitting technique applied to broad-band photometric data. The assumptions underlying this technique appear to be robust (see Littlefair et al. (2008) for a discussion), but the results are of such significance that it is important they are independently verified. In this paper we present time-resolved spectroscopy of the CV SDSS J143317.78+101123.3 (hereafter SDSSJ1433), obtained with the aim of measuring the radial-velocity semi-amplitude of the white dwarf (K_1) and comparing this direct, dynamical measurement of K_1 with that predicted by the light-curve model of Littlefair et al. (2008). The observations were obtained with an electron-multiplying CCD (EMCCD), to the best of our knowledge the first time that such a device has been used for astronomical spectroscopy.

2 OBSERVATIONS AND REDUCTION

SDSSJ1433 is a challenging target as it is faint ($g' = 18.5$) and has a short period (P=78.1 min). This means that spectra taken with a conventional CCD would be swamped by read noise and for this reason we chose to use an Electron Multiplying CCD (Mackay et al. 2001). These devices are able to amplify the signal to such an extent that it renders the readout noise negligible. We observed SDSSJ1433 using

⋆ E-mail: smt@qucam.com (SMT); prguez@ing.iac.es (PRG); vik.dhillon@sheffield.ac.uk (VSD)

Table 1. Full-width at zero intensity, full-width at half maximum, peak-to-peak separation and equivalent width of the Hα emission line shown in Figure 1. The radial velocity semi-amplitude of the WD and the systemic velocity derived in Sections 3.4 and 3.5 are also listed.

FWZI	5000 ± 500 km/s
FWHM	2200 ± 200 km/s
Peak Separation	1300 ± 200 km/s
Equivalent Width	147.2 ± 0.5 Å
K_1	34 ± 4 km/s
γ	75 ± 10 km/s

QUCAM2[1], an EMCCD-based camera mounted on the red arm of the ISIS spectrograph[2] on the 4.2m William Herschel Telescope, La Palma. QUCAM2 employs a 1k × 1k CCD201 detector manufactured by E2V which has a frame-transfer architecture, providing a dead time of only 12 ms between each frame. With the low predicted K_1 it was decided to use the highest dispersion grating available, the R1200R. This provided a wavelength range of 6480–6700Å at a spectral resolution of 32 km s^{-1} (0.7Å) with a slit width of 1″.

On 2008 April 16, we obtained 628 spectra, each of 30s exposure time. The moon was full, the seeing was approximately 0.7–1″ and the sky transparency was variable. A nearby comparison star was also placed on the slit to correct for slit losses and changes in transparency. Arc spectra were taken every 40 minutes for wavelength calibration. No flux standard was observed. This is justified because there was intermittent cloud, we only observed over a narrow wavelength range and we were only interested in extracting velocities from the data.

The spectra were extracted using a simple spatial bin across three windows within each frame covering the target, the reference star and the large area of sky in between. The sky-subtracted spectra were cast into 40 phase bins using the ephemeris of Littlefair et al. (2008), and then corrected for slit losses and transparency variations by dividing by the integrated flux in the comparison star spectra.

3 RESULTS

3.1 Averaged spectrum

Figure 1 shows the average spectrum of SDSSJ1433. The most prominent feature is the broad, double-peaked emission line of Hα. The equivalent and velocity widths of the line are given in Table 1. A weaker feature due to He I λ6678 is also visible. The average spectrum is typical of other eclipsing dwarf novae below the period gap, e.g. WZ Sge (Skidmore et al. 2000).

3.2 Continuum and Hα light curves

We computed the light curve of the continuum by summing the flux in line-free portions of each spectrum. We then fitted and subtracted the continuum of each spectrum, and summed the residual flux in the Hα emission line. The resulting light curves are shown in Figure 2.

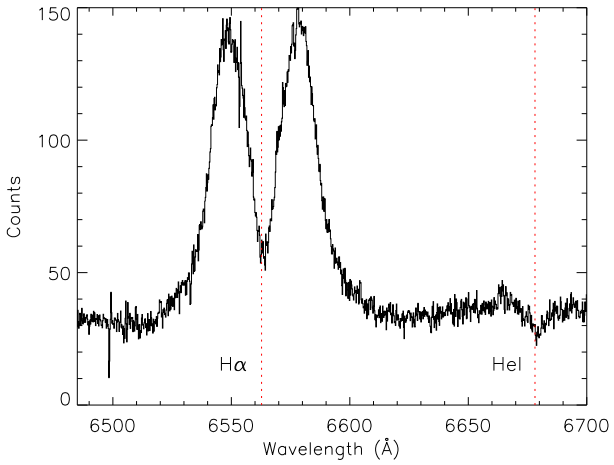

Figure 1. The average spectrum of SDSSJ1433, obtained by combining all 628 spectra.

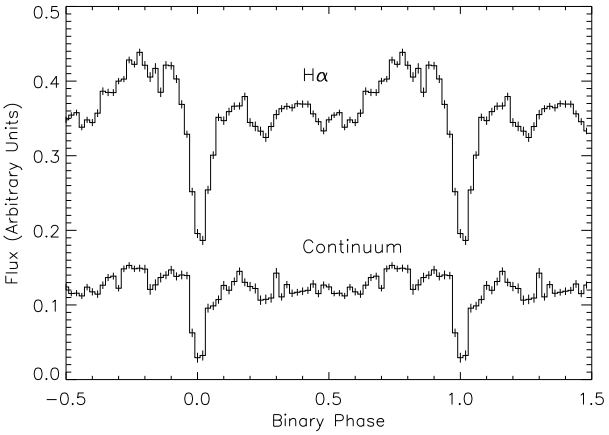

Figure 2. Light curves of the continuum only and the Hα emission line.

Figure 2 shows that Hα experiences broader eclipses than the continuum. The eclipse depth for Hα is $\sim$ 50 %, while for the continuum it is $\sim$ 75 %. This is consistent with Hα being emitted in the optically thin outer parts of the accretion disc and the hotter, optically thick, inner parts of the disc being responsible for the majority of the continuum emission. This picture is confirmed by analysing the light curves of the wings and core of the line separately, which show a deeper eclipse in the former than the latter. An orbital hump prior to eclipse is also apparent in the Hα light curve of figure 2, caused by the changing aspect of emission from the bright spot.

3.3 Trailed spectra and Doppler tomogram

The phase-binned, continuum-subtracted Hα profile is shown as a trail in the lower panel of Figure 3. The primary eclipse around phase 0 is clearly seen, as is the rotational disturbance where the blue peak of the emission line is eclipsed prior to the red peak. The bright spot is clearly visible as an S-wave moving between the two peaks. The orbital modula-

[1] http://www.ing.iac.es/Engineering/detectors/qucam2.html
[2] http://www.ing.iac.es/Astronomy/instruments/isis/index.html

tion of the wings of the emission line can arguably just be made out. There is also evidence for a 'shadow' on the blue edge of the S-wave around phase 0.25 which appears remarkably similar to the models of gas stream overflow computed by Hellier & Robinson (1994).

We computed the Doppler tomogram of the Hα trail using Fourier-filtered back projection (see Marsh (2001) for a review). As expected, the dominant feature is the ring of emission representing the accretion disc which appears to be centred on the expected position of the WD. The bright spot lies on this ring at a velocity intermediate between the free-fall velocity of the gas stream and the Keplerian disc velocity along its path, as observed in some other CVs, e.g. U Gem (Marsh et al. 1990) and WZ Sge (Spruit & Rutten 1998). There is no evidence for emission from the secondary star, nor for asymmetries in the disc emission due to, for example, spiral shocks.

3.4 The diagnostic diagram

The WD primary star orbits with velocity K_1 around the centre of mass of the system, resulting in a periodic Doppler shift of any light it emits. If we imagine the simplified case of an ideal accretion disc centred on the WD with a perfectly symmetric brightness distribution, then the velocity shift of the emission lines generated in the disc will be subject to the same modulation as the WD. If we measure the line centroids and plot them as a function of orbital phase then we should see a sine wave corresponding to the orbital motion of the WD. More realistically, however, if we include the light emitted by the bright spot, we can see that calculated line centroids will, rather than precisely following the WD, be perturbed in the direction of the bright spot. The resultant radial velocity (RV) curve will not only have an excessive amplitude but will also be offset in phase with respect to the true motion of the WD. It is thus important to exclude the bright spot contribution by only examining the light emitted in the wings of the line profile. These emissions correspond to material orbiting within the disc at small radii from the primary star, where they are only minimally contaminated by the bright spot. If the RV curve that we obtain using this technique has the correct phase offset relative to the primary eclipse then we can be confident of an accurate semi-amplitude measurement.

To measure the radial velocities of the wings of the Hα emission line we used the double-Gaussian technique of Schneider & Young (1980). The best signal-to-noise ratio was obtained using a Gaussian width of 350 km s^{-1} and the separation of the Gaussians was then varied between 1500 and 3000 km s^{-1} in steps of 100 km s^{-1} so as to explore annular regions of the accretion disc of decreasing radii. At each Gaussian separation the resulting radial velocities were fitted with a sine function. The phase offset (ϕ_0), semi-amplitude (K), systemic velocity (γ) and fractional error in the amplitude (σ_K/K) of the sine fits were then plotted against the Gaussian separation as a diagnostic diagram (Shafter et al. 1986), as shown in Figure 4. An example of the RV data and sine fit is shown in Figure 5, for a Gaussian separation of 2900 km s^{-1}.

The standard way of obtaining K_1 from a diagnostic diagram is to use the value corresponding to where the σ_K/K curve is at a minimum. If we do this we find a value of $K_1 = 44$km s^{-1}. However, it can be seen that the corresponding value of ϕ_0 is non-zero and declines towards zero at higher Gaussian separations. As pointed out by Marsh (1988), this highlights the main drawback of diagnostic diagrams – the derived K_1-value is noise dependent. The best solution is to use those data points corresponding to the highest Gaussian separations to extrapolate to a K_1-value whose corresponding $\phi_0 = 0$. This requires the construction of a 'Light Centre' diagram (Marsh 1988).

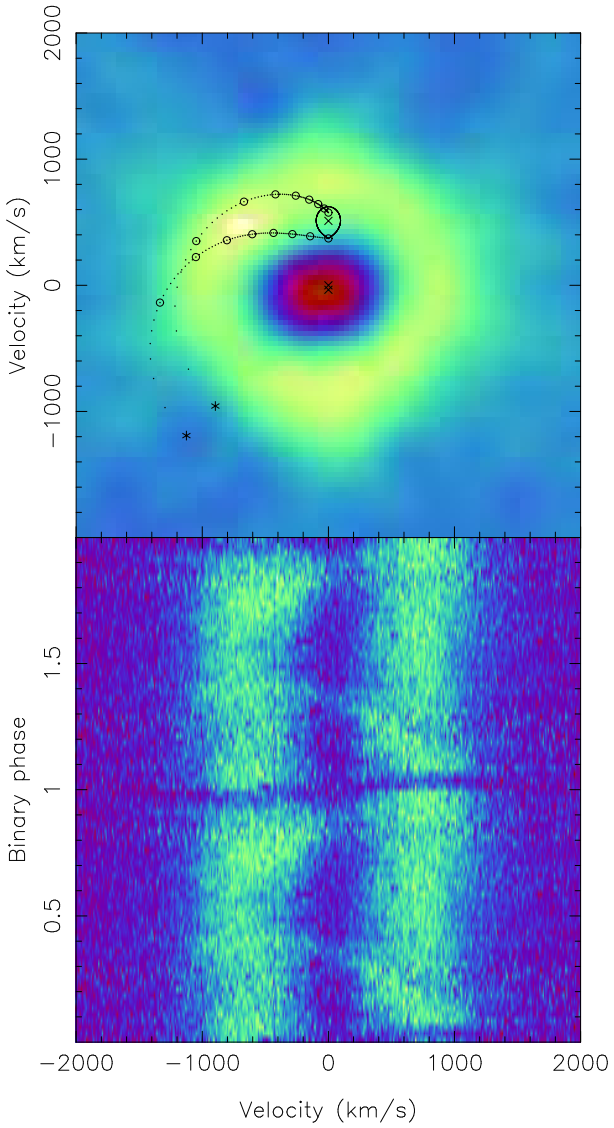

Figure 3. *Bottom:* the Hα trailed spectrum, with two cycles plotted for clarity. *Top:* the Doppler map of Hα. The three crosses represent the centre of mass of the secondary star (upper cross), the system (middle cross) and the WD (lower cross). The Roche lobe of the secondary star, the predicted gas stream trajectory and the Keplerian velocity of the disc along the stream are also shown, calculated assuming the system parameters given in Littlefair et al. (2008). The circular tick marks represent steps of 0.1 L_1 (the inner Lagrangian distance) towards the WD. The asterisks represent the points of closest approach to the WD.

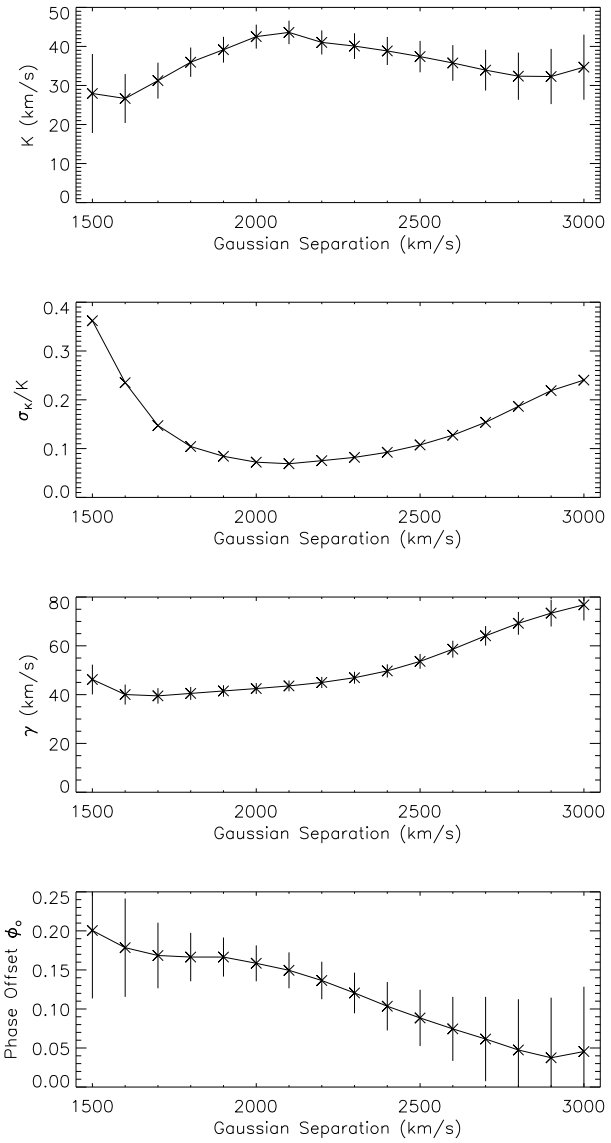

Figure 4. The diagnostic diagram for Hα – see text for details.

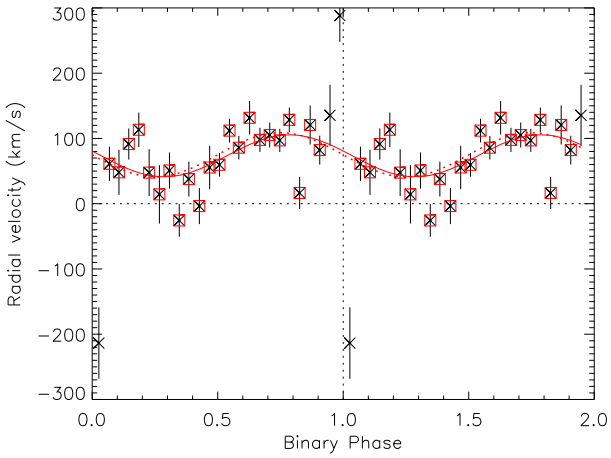

Figure 5. The measured RV data for a Gaussian separation of 2900 km s^{-1} and the resulting sine curve fit (solid line). Only data points marked by a square were included in the fit, i.e. the rotational disturbance was not taken into account. The dashed line shows the sine curve corresponding to the motion of the WD as derived from the light centre diagram presented in Figure 6.

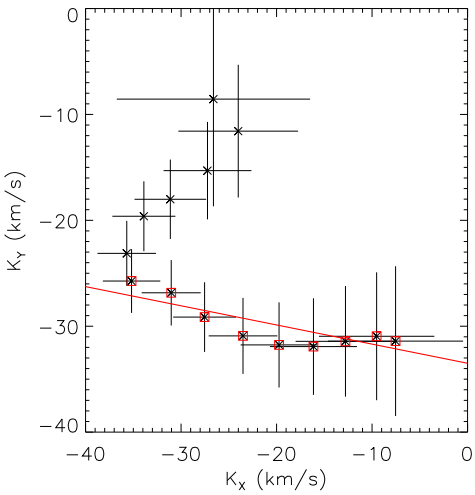

Figure 6. The light centre diagram for Hα, where $-K\sin\phi_0$ is plotted on the abscissa and $-K\cos\phi_0$ on the ordinate. A linear fit to the points marked by squares is also shown, extrapolated to where it intercepts the y-axis. The smallest Gaussian separation corresponds to the top-most point and the largest to the right-most point.

3.5 The light centre method

At no point on the diagnostic diagram does the sine fit have a zero phase offset relative to the WD, although at the extremes of the Hα wings it gets close. The light centre method, described by Marsh (1988), offers a way of extrapolating the data to estimate what the amplitude of the RV curve would be at $\phi_0 = 0$. Just as the Doppler map is a view of an emission line transformed into velocity space, so the light centre diagram, shown in Figure 6, is a velocity space projection of the RV data plotted in the diagnostic diagram.

The radial velocity of the WD can be determined from a light centre diagram by extrapolating a linear fit to the RV data points and reading off the y-axis intercept. To avoid contamination from the bright spot we only included the nine largest Gaussian separations in the linear fit. The resulting intercept is $K_1 = 34 \pm 4$ km s^{-1}, the error quoted corresponding to a combination of statistical error and systematic error due to the exact choice of which points to exclude from the linear fit. The RV curve corresponding to this value of K_1 and $\phi_0 = 0$ is shown as the dashed curve in Figure 5.

We are confident that our measurement of K_1 accurately reflects the motion of the WD in SDSSJ1433 for the following reasons. First, the bottom panel of figure 4 clearly shows a trend to zero phase offset at large Gaussian separations, as one would expect if one is measuring the real radial velocity of the WD in combination with a steadily decreasing contribution from the bright spot. In such instances, the light centre technique has been proven to give reliable results (e.g. IP Peg, Marsh 1988; U Sco, Thoroughgood et al. 2001). Second, the top panel of figure 4 shows that the ra-

dial velocity semi-amplitude is remarkably independent of the Gaussian separation, indicating that our systematic errors are indeed small.

4 CONCLUSIONS

We have measured the radial velocity amplitude, $K_1 = 34 \pm 4$ km s^{-1}, of the WD in the short-period CV SDSSJ1433 by analysing the RV motion of the extreme wings of the Hα emission line. In order to account for the velocity contamination from the conspicuous emission of the bright spot, the light centre technique was used. The measured value of K_1 is consistent with the predicted value of $K_1 = 35 \pm 2$ km s^{-1} from the light-curve fitting technique of Littlefair et al. (2008). Our result therefore supports the validity and accuracy of the purely photometric technique of measuring masses and argues in favour of the presence of a brown-dwarf donor in SDSSJ1433, and by implication in SDSSJ1501 and SDSSJ1507 also. The results presented in this paper also demonstrate that the combination of a large-aperture telescope, an intermediate-resolution spectrograph and an EMCCD is uniquely capable of tackling this type of photon-starved observation.

ACKNOWLEDGMENTS

We thank Tom Marsh for the use of his `MOLLY` and `TRAILER` programs and Stuart Littlefair for useful discussions. The observations were made with the William Herschel Telescope operated on the island of La Palma by the Isaac Newton Group in the Spanish Observatorio del Roque de los Muchachos of the Instituto de Astrofísica de Canarias.

REFERENCES

Hellier C., 2001, Cataclysmic Variable Stars, Springer
Hellier C., Robinson E. L., 1994, ApJ, 431, L107
Littlefair S. P., Dhillon V. S., Marsh T. R., Gänsicke B. T., Southworth J., Watson C. A., 2006, Science, 314, 1578
Littlefair S. P., Dhillon V. S., Marsh T. R., Gänsicke B. T., Southworth J., Baraffe I., Watson C. A., Copperwheat C., 2008, MNRAS, 388, 1582
Mackay C. D., Tubbs R. N., Bell R., Burt D. J., Jerram P., Moody I., 2001, SPIE, 4306, 289
Marsh T. R., 1988, MNRAS, 231, 1117
Marsh T. R., 2001, LNP, 573, 1
Marsh T. R., Horne K., Schlegel E. M., Honeycutt R. K., Kaitchuck R. H., 1990, ApJ, 364, 637
Schneider D. P., Young, P. J., 1980, ApJ, 238, 946
Shafter A. W., Szkody P., Thorstensen J.R., 1986, ApJ, 308, 765
Skidmore W., Mason E., Howell S. B., Ciardi D. R., Littlefair S., Dhillon V. S., 2000, MNRAS, 318, 429
Spruit H. C., Rutten R. G. M., 1998, MNRAS, 299, 768
Thoroughgood, T. D.; Dhillon, V. S.; Littlefair, S. P.; Marsh, T. R. ; Smith, D. A., 2001, MNRAS, 327, 1323
Warner B., 1995, Cataclysmic Variable Stars, CUP

This paper has been typeset from a TEX/ LATEX file prepared by the author.